Dynamical properties of a nonequilibrium quantum dot close to a dissipative quantum phase transition

Chung-Hou Chung

Electrophysics Department, National Chiao-Tung University, HsinChu, Taiwan 300, Republic of China, and Departments of Physics and Applied Physics, Yale University, New Haven, Connecticut 06511, USA

(Received 2 September 2010; revised manuscript received 29 December 2010; published 7 March 2011)

The dynamical decoherence rate and charge susceptibility of a nonequilibrium quantum dot close to a dissipative quantum phase transition are calculated. The setup concerns a resonance-level quantum dot coupled to two spinless fermionic baths with a finite bias voltage and an ohmic bosonic bath representing a dissipative environment. The system is equivalent to an anisotropic Kondo model. As dissipation strength increases, the system at zero temperature and zero bias exhibits a quantum phase transition of the Kosterlitz-Thouless (KT) type between a conducting delocalized phase and an insulating localized phase. Within the nonequilibrium frequency-dependent renormalization group (RG) approach, the finite bias crossover in dynamical decoherence rate and charge susceptibility close to the transition are addressed. The dynamical decoherence rate is found to increase with increasing frequency. In the delocalized phase, it shows a singularity at frequencies equal to positive or negative bias voltage. As the system cross overs to the localized phase, the decoherence rate at low frequencies gets progressively smaller and the singular feature is gradually smeared out, leading to a single linear frequency dependence. The dynamical charge susceptibility at low frequencies shows a dip-to-peak crossover across the transition. Relevance of these results to the experiments is discussed.

DOI: 10.1103/PhysRevB.83.115308 PACS number(s): 72.15.Qm

I. INTRODUCTION

Quantum phase transitions (QPTs)[1,2] due to competing quantum ground states are of fundamental importance in condensed matter physics and have attracted much attention both theoretically and experimentally. Near the transitions, exotic quantum critical properties are realized. In recent years, there has been a growing interest in QPTs in nanosystems.[3–10] Very recently, QPTs have been extended to nonequilibrium nanosystems with a large bias voltage being applied to the setups. Close to QPTs much of the attention has been focused on equilibrium properties, while relatively less is known of the nonequilibrium properties. The key difference between equilibrium and nonequilibrium properties near QPTs is the voltage-induced nonequilibrium decoherence rate, which behaves very differently from that in equilibrium at finite temperatures, leading to distinct nonequilibrium properties near QPTs.

Generic examples of nonequilibrium QPTs in quantum dot devices that have been studied recently include the transport through (i) a dissipative resonance level (spinless quantum dot) at a finite bias voltage in which a dissipative bosonic bath (noise) comes from the environment in the leads,[11] (ii) a spinful quantum dot coupled to two interacting Luttinger liquid leads[12] where the electron interactions can be regarded as an effective ohmic dissipative bosonic bath,[10] and (iii) a single electron transistor (SET) attached to ferromagnetic leads.[13] In particular, for the first two examples, as dissipation (or interaction) strength is increased, both systems can be mapped onto different effective Kondo models. These models exhibit QPT in transport from a conducting delocalized phase (or the Kondo-screened phase in the context of the anisotropic Kondo model) where resonant tunneling dominates to an insulating localized phase (or the ferromagnetic local-moment phase in the anisotropic Kondo model) where the dissipation (or electron-electron interaction) prevails. Similar dissipation driven QPTs have been investigated in various systems.[14,15] To obtain the nonequilibrium transport properties, the authors of Refs. 11 and 12 applied the nonequilibrium frequency-dependent renormalization group (RG) approach[16] in the form of self-consistent scaling equations for frequency-dependent Kondo couplings and the static decoherence rate $\Gamma(V,T,B)$. Though the dynamical nonequilibrium effects in Kondo models have been addressed,[17–19] less is known of the steady-state nonequilibrium decoherence effect on the anisotropic and/or two-channel Kondo models. In this paper, we address the dynamical properties of the nonequilibrium decoherence effect of a dissipative resonance-level quantum dot across the Kosterlitz-Thouless (KT) transition (the first example mentioned above). To obtain the dynamics or the frequency dependence of the decoherence rate, we generalize the frequency-dependent RG approach taken in Refs. 11 and 12 to include the frequency dependence of the decoherence rate self-consistently. The nonequilibrium decoherence rate is directly proportional to the width of the peak in dynamical spin susceptibility. We furthermore investigate the spectral properties of the dynamical decoherence rate close to the QPT and its implications to the dynamical charge susceptibility, which can be measured experimentally. In particular, as the system goes from the delocalized to the localized phase we find the dynamical decoherence rate at small frequencies gets smaller in magnitude and the singular "kink-like" behavior occurring at the frequencies equal to the bias voltage ($\omega = \pm V$) gets smeared out. As the system moves from the delocalized to the localized phase, we find the dynamical (charge) susceptibility shows a dip-to-peak crossover and the smearing of the sharp feature at $\omega \approx \pm V$. The relevance of our results to the experiments is discussed.

II. MODEL HAMILTONIAN

The system we study here is a spin-polarized quantum dot coupled to two Fermi-liquid leads subjected to a noisy ohmic environment. The dissipative environment consists of a collection of harmonic oscillators with ohmic correlation coupled capacitively to the quantum dot.[11] For a dissipative resonant level (spinless quantum dot) model, the quantum phase transition separating the conducting and insulating phases for the level is solely driven by dissipation. The Hamiltonian is given by[11]

$$\begin{aligned} H = & \sum_{k,i=1,2} [\epsilon(k) - \mu_i] c_{ki}^\dagger c_{ki} + t_i c_{ki}^\dagger d + \text{H.c.} \\ & + \sum_r \lambda_r (d^\dagger d - 1/2)(b_r + b_r^\dagger) + \sum_r \omega_r b_r^\dagger b_r \\ & + \epsilon_d (d^\dagger d - 1/2), \end{aligned} \tag{1}$$

where t_i is the hopping amplitude between lead i and the quantum dot, c_{ki} and d are electron operators for the Fermi-liquid leads and the quantum dot, respectively, $\mu_i = \pm V/2$ is the chemical potential (bias voltage) applied on the lead i, and ϵ_d is the energy level of the dot. We assume that the electron spins have been polarized by a strong magnetic field. Here, b_α are the boson operators of the dissipative bath with an ohmic spectral density:[4] $J(\omega) = \sum_r \lambda_r^2 \delta(\omega - \omega_r) = \alpha\omega$ with α being the strength of the dissipative boson bath.

Through similar bosonization and refermionization procedures as in equilibrium,[3,4,6,7] the above model is mapped onto an equivalent anisotropic Kondo model in an effective magnetic field ϵ_d with the effective left L and right R Fermi-liquid leads.[11] The effective Kondo model takes the form

$$\begin{aligned} H_K = & \sum_{k,\gamma=L,R,\sigma=\uparrow,\downarrow} [\epsilon_k - \mu_\gamma] c_{k\gamma\sigma}^\dagger c_{k\gamma\sigma} \\ & + (J_\perp^1 s_{LR}^+ S^- + J_\perp^2 s_{RL}^+ S^- + \text{H.c.}) \\ & + \sum_{\gamma=L,R} J_z s_{\gamma\gamma}^z S^z + h S_z, \end{aligned} \tag{2}$$

where $c_{kL(R)\sigma}^\dagger$ is the electron operator of the effective lead $L(R)$ with spin σ. Here, the spin operators are related to the electron operators on the dot by $S^+ = d^\dagger$, $S^- = d$, and $S^z = d^\dagger d - 1/2 = n_d - 1/2$, where $n_d = d^\dagger d$ describes the charge occupancy of the level. The spin operators for electrons in the effective leads are $s_{\gamma\beta}^\pm = \sum_{\alpha,\delta,k,k'} (1/2) c_{k'\gamma\alpha}^\dagger \sigma_{\alpha\delta}^\pm c_{k'\beta\delta}$, the transverse and longitudinal Kondo couplings are given by $J_\perp^{1(2)} \propto t_{1(2)}$ and $J_z \propto (1/2)(1 - 1/\sqrt{2\alpha^*})$, respectively, and the effective bias voltage is $\mu_\gamma = \pm\frac{V}{2}\sqrt{1/(2\alpha^*)}$, where $1/\alpha^* = 1 + \alpha$. Note that $\mu_\gamma \to \pm V/2$ near the transition ($\alpha^* \to 1/2$ or $\alpha \to 1$) where the above mapping is exact.[20] The spin operator of the quantum dot in the effective Kondo model, $\vec{S}$, can also be expressed in terms of the spinful pseudofermion operator f_σ: $S_{i=x,y,z} = f_\alpha^\dagger \sigma_{i=x,y,z}^{\alpha\beta} f_\beta$. In the Kondo limit where only the singly occupied fermion states are physically relevant, a projection onto the singly occupied states is necessary in the pseudofermion representation.[11,16] This can be achieved by introducing the Lagrange multiplier λ so that $Q = \sum_\gamma f_\gamma^\dagger f_\gamma = 1$.[21,22] In equilibrium, the above anisotropic Kondo model exhibits the KT transition from a delocalized phase with a finite conductance $G \approx \frac{1}{2\pi\hbar}$ ($e = \hbar = 1$) for $J_\perp + J_z > 0$ to a localized phase for $J_\perp + J_z \leqslant 0$ with vanishing conductance. The distinct profile in nonequilibrium transport near the localized-delocalized KT transition has been addressed in Ref. 11. Below we will turn our attention to the dynamical decoherence rate and charge susceptibility of the quantum dot close to the transition.

III. NONEQUILIBRIUM FREQUENCY-DEPENDENT RG FORMALISM

The nonequilibrium frequency-dependent RG approach is based on the generalization of the previous RG approach in Ref. 16 for the nonequilibrium Kondo model. The frequency-dependent RG scaling equations for the effective Kondo couplings in the Keldysh formulation are given by[16]

$$\begin{aligned} \frac{\partial g_z(\omega)}{\partial \ln D} &= -\sum_{\beta=-1,1} \left[g_\perp \left(\frac{\beta V}{2} \right) \right]^2 \Theta_{\omega + \frac{\beta V}{2}}, \\ \frac{\partial g_\perp(\omega)}{\partial \ln D} &= -\sum_{\beta=-1,1} g_\perp \left(\frac{\beta V}{2} \right) g_z \left(\frac{\beta V}{2} \right) \Theta_{\omega + \frac{\beta V}{2}}, \end{aligned} \tag{3}$$

where $g_\perp(\omega) = N(0) J_\perp^1 = N(0) J_{\perp\sigma}^2$ and $g_z(\omega) = N(0) J_z$ are dimensionless frequency-dependent Kondo couplings with $N(0)$ being density of states per spin of the conduction electrons (where we assume symmetric hopping, $t_1 = t_2 = t$). Here, $\Theta_\omega = \Theta(D - |\omega + i\Gamma(\omega)|)$ (with $D < D_0$ being the running cutoff) comes from the leading logarithmic corrections for the Kondo vertex function originated from the product of the Keldysh component of the lead electron Green function $G_\alpha^K(\omega)$ with the real part of the retarded or advanced dressed pseudofermion propagator $\text{Re}(\tilde{G}_f^{R/A})$:[23]

$$\begin{aligned} G_\alpha^K(\omega) &= -2\pi i \tanh \left(\frac{\omega - \mu_\alpha}{2T} \right) N_0 \Theta(D_0 - |\omega|), \\ \tilde{G}_{f\sigma}^R(\omega) &= \frac{1}{\omega - \Sigma_\sigma^R(\omega)} = \left[\tilde{G}_{f\sigma}^A(\omega) \right]^*, \end{aligned} \tag{4}$$

where $\Sigma_\sigma^R(\omega) = \text{Re}[\Sigma_\sigma^R(\omega)] + \frac{i}{2}\Gamma_\sigma(\omega)$ is the impurity self-energy (defined below) with the imaginary part being the dynamical decoherence rate $\Gamma_\sigma(\omega)$, and $N_0 = \frac{1}{2D_0}$. Note that we generalize the approach in Ref. 16 by allowing the frequency dependence for the decoherence rate. More precisely, the decoherence rate Γ in Ref. 16 corresponds to $\Gamma(\omega = 0)$ here. At $T = 0$, the above correction can be approximated by the Θ function in the RG equations shown above. Also, the dynamical decoherence (dephasing) rate $\Gamma_\sigma(\omega)$ at finite bias, which serves as a cutoff to the RG flow of $g_{\perp,z}(\omega)$,[16] is determined self-consistently along with the RG equations for the Kondo couplings. Note that in general $\Gamma_\sigma(\omega)$ depends on the impurity spin σ; however, in the absence of magnetic fields as we consider here, we have the spin symmetry and hence we have $\Gamma_\uparrow(\omega) = \Gamma_\downarrow(\omega) = \Gamma(\omega)$. Here, the frequency-dependent decoherence rate $\Gamma(\omega)$ is obtained from the imaginary part of the pseudofermion self-energy via second-order renormalized

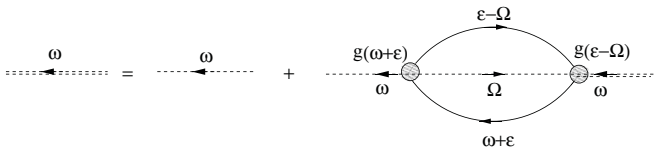

FIG. 1. Diagram for the pseudofermion self-energy. The double-dashed line represents the dressed pseudofermion propagator; the single-dashed lines denote the bare pseudofermion propagators. The solid lines are the conduction electron propagators. The small shaded circles denote the Kondo interaction vertex, and $g(\omega+\epsilon)$ and $g(\epsilon-\Omega)$ represent the frequency-dependent renormalized dimensionless Kondo couplings defined in the text.

perturbation theory[21] (see Fig. 1):

$$\Gamma_\sigma(\omega) = \mathrm{Im}[\Sigma_\sigma(\omega)] = i\big(\Sigma_\sigma^R - \Sigma_\sigma^A\big),$$
$$i\Sigma_\sigma^{R(A)}(\omega) = \sum_{\sigma',\alpha,\beta=L,R} \frac{\theta_{\sigma\sigma'}}{16}\int \frac{d\epsilon}{2\pi} g_{\alpha\beta}(\omega+\epsilon) \times \chi_{cf,\sigma'}^{<(>),\alpha\beta}(\epsilon) G_\beta^{>(<)}(\epsilon+\omega), \tag{5}$$

where $\sigma,\sigma' = \uparrow, \downarrow$, $g_{LR} \equiv g_\perp$, $g_{LL/RR} \equiv g_z$, $\theta_{\sigma\sigma'}$ is the tensor associated with the product of the Pauli matrices:[16]

$$\theta_{\gamma\gamma'} = \frac{1}{2}\sum_{\sigma,\sigma'} \tau^i_{\sigma\sigma'}\tau^i_{\gamma\gamma'}\tau^j_{\sigma'\sigma}\tau^j_{\gamma'\gamma} = \delta_{\gamma\gamma'} + 2\tau^1_{\gamma'\gamma}, \tag{6}$$

and $\chi_{cf,\sigma}^{<(>),\alpha\beta}$ reads

$$\chi_{cf,\sigma}^{<(>),\alpha\beta}(\epsilon) = \int \frac{d\Omega}{2\pi} g_{\beta\alpha}(\epsilon-\Omega)[\hat{G}_{\alpha\sigma}(\epsilon+\Omega)\hat{G}_{f\sigma}(\Omega)]^{<(>)}, \tag{7}$$

where $\hat{G}$ is the Green's function in 2×2 Keldysh space and its lesser and greater Green's functions are related to its retarded, advanced, and Keldysh components by

$$G^< = (G^K - G^R + G^A)/2,$$
$$G^> = (G^K + G^R - G^A)/2. \tag{8}$$

Specifically, the lesser and greater components of the Green's function of the conduction electron in the leads and of the quantum dot (impurity) are given by (in the absence of a magnetic field)

$$G^<_{L/R}(\epsilon) = iA_c(\epsilon) f_{\epsilon-\mu_{L/R}},$$
$$G^>_{L/R}(\epsilon) = iA_c(\epsilon)(1 - f_{\epsilon-\mu_{L/R}}),$$
$$G^<_{f\sigma}(\epsilon) = 2\pi i\delta(\epsilon) n_{f\sigma}(\epsilon),$$
$$G^>_{f\sigma}(\epsilon) = 2\pi i\delta(\epsilon)[n_{f\sigma}(\epsilon) - 1], \tag{9}$$

where $A_c(\epsilon) = 2\pi N_0^2\Theta(D_0-\epsilon)$ is the density of states of the leads and $n_{f\sigma}(\epsilon) = f_\sigma^\dagger f_\sigma$ is the occupation number of the pseudofermion which obeys $n_{f\uparrow} + n_{f\downarrow} = 1$, $n_{f\sigma}(\epsilon\to 0) = 1/2$ in the delocalized phase and $n_{f\uparrow}(\epsilon\to 0)\to 0$, $n_{f\downarrow}(\epsilon\to 0)\to 1$ in the localized phase.[11,22] Here, the pseudofermion occupation number $n_{f\sigma}$ and the occupation number on the dot, n_d, are related via $\langle n_{f\uparrow} - n_{f\downarrow}\rangle = \langle n_d\rangle - 1/2$. Also, $f_{\omega-\mu_{L/R}}$ is the Fermi function of the L/R lead given by $f_{\omega-\mu_{L/R}} = 1/(1+e^{(\omega-\mu_{L/R})/k_BT})$. After simplifications, we have

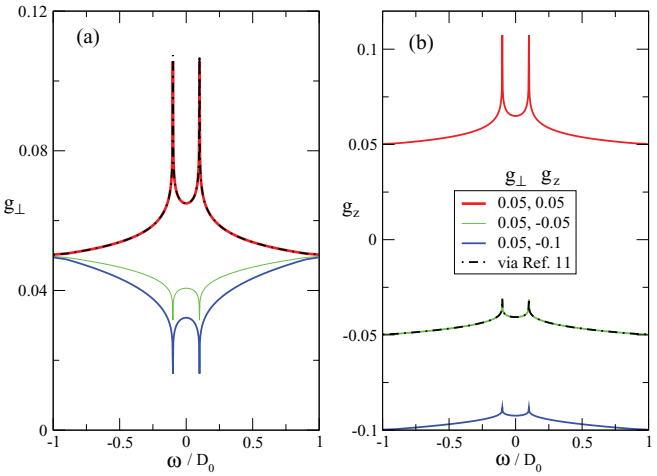

FIG. 2. (Color online) Frequency-dependent Kondo couplings of a dissipative resonant level model at zero temperature for (a) $g_\perp(\omega)$ and (b) $g_z(\omega)$ across the localized-delocalized transition for different bare Kondo couplings (in unit of D_0) via our generalized frequency-dependent RG approach (solid lines) and the approach in Ref. 11 (dot-dashed lines). We have set $V = 0.2D_0$, where $D_0 = 1$ for all the figures.

$$\chi_{cf,\sigma}^{<,\alpha\beta}(\epsilon) = 2\pi i g_{\beta\alpha}(\epsilon)A_c(\epsilon)[1 - n_{f\sigma}(\epsilon)]f_{\epsilon-\mu_\alpha},$$
$$\chi_{cf,\sigma}^{>,\alpha\beta}(\epsilon) = 2\pi i g_{\beta\alpha}(\epsilon)A_c(\epsilon)n_{f\sigma}(\epsilon)(1 - f_{\epsilon-\mu_\alpha}). \tag{10}$$

The dynamical decoherence rate is therefore given by

$$\Gamma(\omega) = \frac{3}{4\pi}\int d\epsilon\, g_\perp(\epsilon+\omega)g_\perp(\epsilon)\big[f_{\epsilon-\mu_L}\big(1 - f_{\epsilon+\omega-\mu_R}\big)\big] + g_z(\epsilon+\omega)g_z(\epsilon)\big[f_{\epsilon-\mu_L}\big(1 - f_{\epsilon+\omega-\mu_L}\big)\big] + (L\to R). \tag{11}$$

The frequency-dependent RG approach here is accomplished by self-consistently solving the RG scaling Eq. (3) subject to Eq. (11). The solutions at zero temperature for $g_\perp(\omega)$ and $g_{\sigma,z}(\omega)$ across the transition are shown in Fig. 2.[11]

Here, we make the following remarks on our RG approach: First, the approach used in this paper is the generalized version of the previous frequency-dependent RG approach in Ref. 16: We include the frequency dependence for the decoherence rate, while in Ref. 16 it is fixed at zero frequency. Similar to Ref. 16, we self-consistently solve the frequency-dependent decoherence rate within renormalized perturbation theory along with the RG scaling equations for the Kondo couplings. Though a more rigorous functional renormalization group (FRG) approach has been developed in Ref. 23 where the decoherence rate is determined entirely within the framework of the FRG, our approach is a well-justified procedure: It includes all the leading logarithmic corrections for the Kondo couplings within renormalized perturbation theory where the renormalized Kondo couplings are obtained from the RG procedure (rather than from the bare Kondo couplings). As shown in Refs. 16 and 24, the results via this approach are in excellent agreement with the recent experiments on nonequilibrium transport in Kondo dot systems. In the present work, we take the generalized version of this well-justified

approach by including the frequency dependence in the decoherence rate. This allows us to extract the dynamical properties of the decoherence rate.

Second, our nonequilibrium RG approach is controlled not only in the localized phase for all values of V but also in the delocalized phase provided $V \gg T_k$. In the localized phase and for $V \to 0$, under RG, $J_\perp^{1,2}$ flow to 0 and $J_z^{1,2}$ flow to a small fixed-point value. Hence, all Kondo couplings are in the perturbative regime under RG. In the delocalized phase, our RG approach is uncontrolled for $V \to 0$ as Kondo couplings are divergent. Nevertheless, in this paper we restrict ourselves to the parameter range $V \gg T_k \propto e^{-1/|\alpha-\alpha_c|}$, where the large bias voltage leads to a cutoff for the divergent RG flows of the Kondo couplings, keeping the renormalized Kondo couplings in the perturbative regime, $g_{\perp,z}(\omega) \ll 1$.[16] Therefore, similar to Refs. 16,21, and 24 where the frequency-dependent RG approach is applied to study the nonequilibrium transport through a Kondo dot in the limit of large bias voltage ($V \gg T_k$), our approach is still a controlled method in the delocalized (or equivalently the Kondo) phase.

As the system moves from the delocalized to localized phase transition, the features in $g_\perp(\omega)$ at $\omega = \pm V/2$ undergo a crossover from symmetric double peaks to symmetric double dips, while the symmetric two peaks in $g_z(\omega = \pm V/2)$ still remain peaks. We find the above results based on the generalized frequency-dependent RG approach are in good agreement with the previous heuristic methods,[11,16] which provides us with an independent check on the previous results in Refs. 11 and 16. Note that from previous approaches in Refs. 11, 12, and 16 the decoherence rate was taken approximately as $\Gamma(\omega = 0)$; we now generalize this Γ by including the frequency dependence. This generalization improves the previous RG formalism and it also provides us with more features in the dynamical quantities across the transition, such as in dynamical charge susceptibility.

It is worthwhile mentioning that unlike the equilibrium RG at finite temperatures where RG flows are cut off by temperature T, here in nonequilibrium the RG flows will be cut off by the decoherence rate Γ, a much lower energy scale than V, $\Gamma \ll V$. This explains the dips (peaks) structure in $g_{\perp(z)}(\omega)$ in Fig. 2 . In contrast, the equilibrium RG will lead to approximately frequency-independent couplings [or "flat" functions $g_\perp(\omega) \approx g_{\perp,z}(\omega = 0)$]. In the absence of field ($h = 0$), $g_{\perp,(z)}(\omega)$ show dips (peaks) at $\omega = \pm V/2$. We use the solutions of the frequency-dependent Kondo couplings $g_{\perp,z\sigma}(\omega)$ to compute the dynamical decoherence rate and charge susceptibility of the resonance level near the delocalized-localized quantum phase transition.

IV. DYNAMICAL DECOHERENCE RATE AND CHARGE SUSCEPTIBILITY

We have solved for the dynamical decoherence rate $\Gamma(\omega)$ at zero temperature self-consistently along with the RG equations (3) subject to Eq. (11). The results are shown in Fig. 3. The general trend we find is that $\Gamma(\omega)$ increases with increasing frequency, while it decreases in magnitude at low frequencies $|\omega| < V$ as the system cross overs from the delocalized to the localized phase. In addition, in the delocalized phase, it shows a singular kink-like behavior at

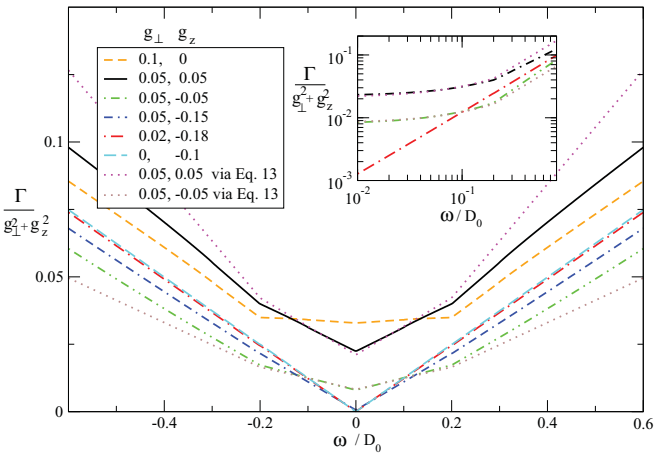

FIG. 3. (Color online) $\Gamma(\omega)$ (rescaled to $g_\perp^2 + g_z^2$ with $g_{\perp,z}$ being the bare Kondo couplings in units of D_0) vs ω at zero temperature across the delocalized-localized KT transition. The inset shows the log-log plot of $\Gamma(\omega)$ vs ω. The bias voltage is fixed at $V = 0.2D_0$. Here, $D_0 = 1$ for all the figures.

frequencies $\omega = \pm V$, separating two different behaviors for $|\omega| > V$ and $|\omega| < V$. The curves of $\Gamma(\omega)$ for $|\omega| < V$ are closer to the linear behavior than those for $|\omega| > V$. As the system moves to the localized phase, $\Gamma(\omega)$ for both $|\omega| < V$ and $|\omega| > V$ gradually changes its slopes or curvatures and finally merges into a single linear behavior deep in the localized phase (see Fig. 3).

To understand the above qualitative features, it proves useful to simplify the zero-temperature dynamical decoherence rate in Eq. (11) to the following form:

$$\begin{aligned}\Gamma(\omega) = {} & \frac{3}{4\pi}\left[\int_{-V/2-\omega/2}^{V/2+\omega/2} + \int_{-V/2+\omega/2}^{V/2-\omega/2}\right] d\epsilon \\ & \times g_\perp(\epsilon - \omega/2) g_\perp(\epsilon + \omega/2) \\ & + \frac{3}{4\pi}\left[\int_{V/2-\omega/2}^{V/2+\omega/2} + \int_{-V/2-\omega/2}^{-V/2+\omega/2}\right] d\epsilon \\ & \times g_z(\epsilon - \omega/2) g_z(\epsilon + \omega/2) \quad (|\omega| < V), \\ \Gamma(\omega) = {} & \frac{3}{4\pi}\left[\int_{-V/2-\omega/2}^{V/2+\omega/2} + \int_{V/2-\omega/2}^{-V/2+\omega/2}\right] d\epsilon \\ & \times g_\perp(\epsilon - \omega/2) g_\perp(\epsilon + \omega/2) \\ & + \frac{3}{4\pi}\left[\int_{V/2-\omega/2}^{V/2+\omega/2} + \int_{-V/2-\omega/2}^{-V/2+\omega/2}\right] d\epsilon \\ & \times g_z(\epsilon - \omega/2) g_z(\epsilon + \omega/2) \quad (|\omega| > V). \end{aligned} \tag{12}$$

In the "flat" (or in the "equilibrium form") approximation where $g_{\perp,z}(\omega)$ are treated as flat functions $g_{\perp,z}(V,\omega = 0) \approx g_{\perp,z}(V = T)$ with T being temperature,[11] Eq. (12) can be simplified as the following linear behaviors:

$$\begin{aligned}\Gamma^e(\omega) &= \frac{3}{2\pi}\left[V g_\perp^2(0) + \omega g_z^2(0)\right] \quad (|\omega| < V), \\ \Gamma^e(\omega) &= \frac{3}{2\pi}\omega\left[g_\perp^2(0) + g_z^2(0)\right] \quad (|\omega| > V). \end{aligned} \tag{13}$$

As shown in Fig. 3, the above approximated form $\Gamma^e(\omega)$ agrees well with $\Gamma(\omega)$ for $|\omega| < V$, but it shows deviation from $\Gamma(\omega)$ for $|\omega| > V$. The approximated form $\Gamma^e(\omega)$ exhibits two linear

behaviors with different slopes for $|\omega| < V$ and $|\omega| > V$, respectively, leading to a kink-like singularity at $\omega = \pm V$. As the system moves from the delocalized to the localized phase, the ratio $g_\perp(0)/g_z(0)$ becomes progressively smaller, leading to suppressions of the two slopes. Finally, as the system moves deeply in the localized phase, these two lines merge into a single line since $|g_\perp(0)| \ll |g_z(0)|$ there. The qualitative behaviors of $\Gamma^e(\omega)$ can explain the overall monotonically increasing trend of $\Gamma(\omega)$ with increasing frequency as well as the decreasing trend of $\Gamma(|\omega| < V)$ as the system moves from the delocalized to the localized phase.

When the full frequency dependence of $g_{\perp,z}(\omega)$ is considered, we find that $\Gamma(\omega)$ deviates from the perfect linear behavior in $\Gamma^e(\omega)$ (see Fig. 3). Furthermore, in the delocalized phase, the correction to the linear behavior, $\Gamma(\omega) - \Gamma^e(\omega)$, is more noticeable in the high-frequency regime ($|\omega| > V$) than in the low-frequency regime ($|\omega| < V$) (see Fig. 3). This comes as a result of the wider range in energy ϵ to be integrated over in Eq. (12) for $|\omega| > V$, which accumulates more deviations from the flat approximation due to the dip-peak frequency dependence of $g_{\perp,z}(\omega)$. As the system moves to the localized phase, $\Gamma(|\omega| > V)$ becomes closer to the linear behavior as a result of the flatter $g_z(\omega)$ in the localized phase. Meanwhile, we find that the correction to the linear behavior as well as the singularities at $\omega = \pm V$ for $\Gamma(\omega)$ are logarithmic in nature in the delocalized phase ($g_\perp = 0.05 D_0 = g_z$) and at the KT transition ($g_\perp = 0.05 D_0 = -g_z$), while they are power law in nature for $|g_\perp| \neq |g_z|$. This comes as a result of the logarithmic and power-law behaviors for $g_{\perp,z}(\omega)$ in these limits, respectively.[11] Note also that for $|\omega| > V$ we find $\Gamma(\omega) < \Gamma^e(\omega)$ in the delocalized phase, while the opposite holds in the localized phase. This can be understood as follows: In the delocalized phase $|g_{\perp(z)}(\omega)| < |g_{\perp(z)}(0)|$ for the majority of the frequencies (except for ω very close to $\pm V/2$), leading to a smaller value of $\Gamma(\omega)$ compared to $\Gamma^e(\omega)$, while the opposite is true in the localized phase. We have checked numerically that $\Gamma(\omega = 0)$ obtained here indeed reproduces the frequency-independent decoherence rate Γ obtained in Ref. 11.

The effect of the dynamical decoherence rate can be measured experimentally via dynamical charge susceptibility $\chi_c(\omega)$: $\mathrm{Im}\big(\chi_c(\omega)\big) \propto \lim_{\epsilon_d \to 0} d n_d(\omega)/d\epsilon_d$ with $\epsilon_d \propto (N - 1/2)$ being the effective magnetic field measuring the deviations of N electrons on the dot from the charge degeneracy point. Here, $\chi_c(\omega)$ is the Fourier-transformed charge susceptibility defined as

$$\chi_c(t) \equiv i\theta(t)\langle[\big(n_d(t) - 1/2\big), \big(n_d(0) - 1/2\big)]\rangle. \tag{14}$$

Experimentally, the dynamical charge susceptibility can be measured by the capacitance line shape in an ac field near the charge degeneracy point via the high-sensitivity charge sensor in the SET connected to the dot.[25] The decoherence rate $\Gamma(\omega = 0)$ here corresponds to the broadening of the resonance peak in the imaginary part of $\chi_c(\omega)$. We have calculated $\chi_c(\omega)$ at zero temperature based on renormalized second-order perturbation theory (see the diagram in Fig. 4). From the mapping mentioned above, the dynamical charge susceptibility $\chi_c(\omega)$ is related to the z component of the effective spin-spin correlation function χ_{zz} in the effective Kondo model through

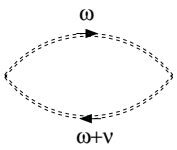

FIG. 4. Diagram for the charge susceptibility. The dressed pseudofermion propagator (double-dashed line) is calculated via the diagram in Fig. 1.

$$\begin{aligned}\chi_c(t) &\equiv -i\theta(t)\langle[\big(n_d(t) - 1/2\big), \big(n_d(0) - 1/2\big)]\rangle \\ &\equiv \chi_{zz}(t),\end{aligned} \tag{15}$$

$$\chi_{zz}(t) \equiv -i\theta(t)\langle[S_z(t), S_z(0)]\rangle.$$

By taking the Fourier transform of $\chi_{zz}(t)$ and evaluating the diagram in Fig. 4, the imaginary part of $\chi_{zz}(\omega)$, $\chi_{zz}''(\omega) = \mathrm{Im}\big(\chi_{zz}(\omega)\big)$ is given by

$$\begin{aligned}\chi_{zz}''(\omega) = \int \frac{d\epsilon}{2\pi} \sum_{\sigma=\uparrow,\downarrow} [&\bar{G}^{<}_{f,\sigma}(\omega + \epsilon)\bar{G}^{>}_{f,\sigma}(\epsilon) \\ &- \bar{G}^{>}_{f,\sigma}(\omega + \epsilon)\bar{G}^{<}_{f,\sigma}(\epsilon)],\end{aligned} \tag{16}$$

where $\bar{G}^{>(<)}$ denote the greater (lesser) components of the dressed pseudofermion Green's functions

$$\begin{aligned}\bar{G}^{<}_{f\sigma}(\omega) &= 2\pi i n_{f\sigma}(\omega)\bar{A}_{f\sigma}(\omega), \\ \bar{G}^{>}_{f\sigma}(\omega) &= 2\pi i (n_{f\sigma}(\omega) - 1)\bar{A}_{f\sigma}(\omega), \\ \bar{A}_{f\sigma}(\omega) &= \mathrm{Im}\left[\frac{1}{\omega + \Sigma_{f\sigma}(\omega) + i\eta}\right],\end{aligned} \tag{17}$$

and where $n_{f\sigma}(\omega)$ is the nonequilibrium occupation number determined self-consistently by the quantum Boltzmann equation:[21]

$$n_\sigma(\omega) = [1 - \Sigma^{>}_\sigma(\omega)/\Sigma^{<}_\sigma(\omega)]^{-1} \tag{18}$$

with $\Sigma^{>(<)}_\sigma(\omega)$ as defined in Ref. 22. The resulting expression for $\chi_{zz}(\omega)$ at $T = 0$ is given by

$$\chi_{zz}''(\omega) = \frac{\Gamma(\omega)}{\omega^2 + \Gamma^2(\omega)} \times [1 - 2n_{f\uparrow}(\omega)], \tag{19}$$

where $n_{f\uparrow}(\omega)$ is given by[21]

$$\begin{aligned}n_{f\uparrow}(\omega) &\approx \frac{1}{2}\frac{g_\perp^2(0)(V - \omega)}{2g_z^2(0)\omega + g_\perp^2(0)(V + \omega)} \quad (0 < \omega < V) \\ n_{f\uparrow}(\omega) &\approx \frac{1}{2}\frac{g_\perp^2(0)(V - \omega - 2g_z^2\omega)}{g_\perp^2(0)(V + \omega)} \quad (-V < \omega < 0).\end{aligned} \tag{20}$$

Note that we have neglected the vertex correction[21] in the calculation for $\chi_{zz}(\omega)$ as it gives only a subleading correction to Eq. (19).

As shown in Fig. 5, in the delocalized phase, $\chi_{zz}(\omega \to 0) \propto \omega \to 0$, while $\chi_{zz}(\omega \to 0) \to 1/\omega$ in the localized phase. Hence, as the system cross overs from the delocalized to the localized phase $\chi_{zz}''(\omega)$ shows a dip-to-peak crossover for small ω. This behavior can be understood as follows. In

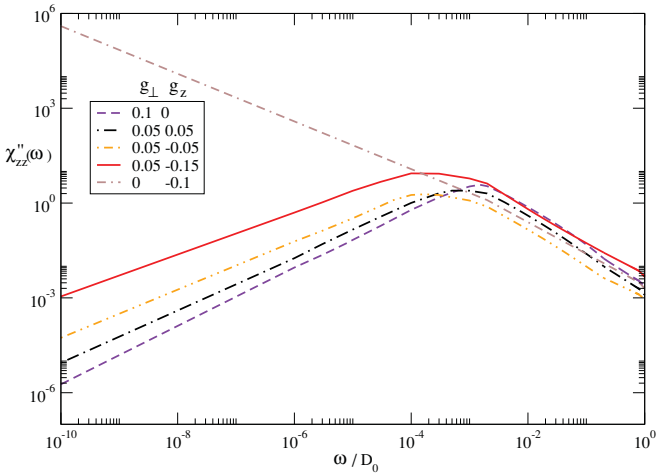

FIG. 5. (Color online) $\chi''_{zz}(\omega)$ vs ω at zero temperature across the localized-delocalized KT transition. The bias voltage is fixed at $V = 0.2D_0$. Here, the bare Kondo couplings $g_{\perp,z}$ are in unit of $D_0 = 1$.

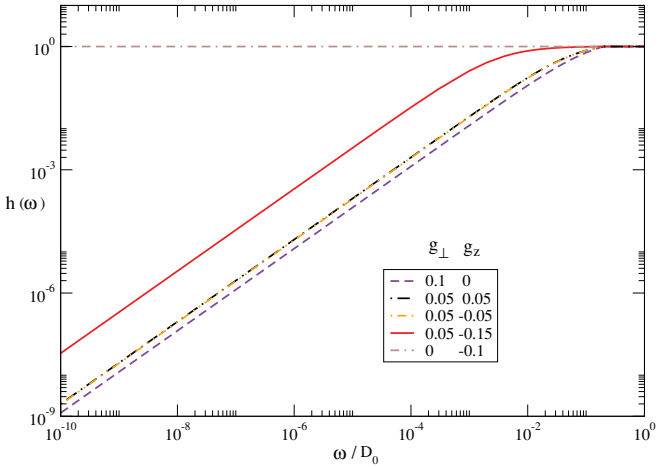

FIG. 6. (Color online) The fluctuation-dissipation ratio $h(\omega)$ vs ω at zero temperature across the localized-delocalized KT transition. The bias voltage is fixed at $V = 0.2D_0$. Here, the bare Kondo couplings $g_{\perp,z}$ are in units of $D_0 = 1$.

the delocalized (Kondo-screened) phase, the effective local spin gets Kondo screened in the low-energy scale; therefore, the spin susceptibility should vanish. On the other hand, in the localized (ferromagnetic) phase, the unscreened free spin gives rise to the Curie-law susceptibility $\chi''_{zz}(\omega) \propto 1/\omega$ at low energies. Meanwhile, in the delocalized phase, we find a a kink-like singular behavior in $\chi''_{zz}(\omega)$ at $\omega = V$, coming from the singular behaviors of both $\Gamma(\omega = V)$ [see Eq. (3)] and the factor $1 - 2n_{f\uparrow}$ in $\chi''_{zz}(\omega = V)$ [see Eq. (19) and discussions below]. However, this singularity gets smeared out as the system cross overs to the localized phase. We have checked that our results for $\chi''_{zz}(\omega)$ in the isotropic Kondo limit agree qualitatively well with those in Refs. 17 and 26. For $\omega \gg V$, we find Curie-like susceptibility $\chi''_{zz}(\omega) \propto 1/\omega$ in both localized and delocalized phases, following Eqs. (19) and (13).

Our results can be furthermore linked to the equilibrium and nonequilibrium fluctuation-dissipation theorem.[17–19,26,27] To do so, it is useful to define the dynamical fluctuation-dissipation ratio $h(\omega)$:

$$h(\omega) = \frac{\chi''_{zz}(\omega)}{S_{zz}(\omega)}, \tag{21}$$

where $S_{zz}(\omega)$ is the Fourier-transformed longitudinal spin-spin correlation function with its real-time form given by

$$S_{zz}(t) = \tfrac{1}{2}\langle\{S_z(t), S_z(0)\}\rangle. \tag{22}$$

The dynamical spin-spin correlation function $S_{zz}(\omega)$ is given by

$$S_{zz}(\omega) = \int \frac{d\epsilon}{2\pi} \sum_{\sigma=\uparrow,\downarrow} [\bar{G}^{<}_{f,\sigma}(\omega+\epsilon)\bar{G}^{>}_{f,\sigma}(\epsilon) + \bar{G}^{>}_{f,\sigma}(\omega+\epsilon)\bar{G}^{<}_{f,\sigma}(\epsilon)]. \tag{23}$$

Carrying out similar calculations as in $\chi''_{zz}(\omega)$, we find the fluctuation-dissipation ratio $h(\omega)$ reads

$$h(\omega) = 1 - 2n_{f\uparrow}(\omega), \tag{24}$$

where $n_{f\uparrow}(\omega)$ is defined in Eq. (20). In equilibrium, the ratio $h(\omega) = h^0(\omega)$ respects the fluctuation-dissipation theorem,[17–19,26] given by $h^0(\omega) = 1 - 2n^0_f(\omega) = \tanh(\beta\omega/2)$, where $n^0_f(\omega) = \frac{1}{e^{\beta\omega}+1}$ is the Fermi function for pseudofermions in equilibrium. At $T = 0$ ($\beta \to \infty$), we have $h^0(\omega > 0) = 1$, the signature of the equilibrium fluctuation-dissipation theorem at $T = 0$. In nonequilibrium and at $T = 0$, however, we find in general a deviation of $h(\omega)$ in the delocalized phase from the equilibrium fluctuation-dissipation theorem: $h(\omega) < 1$ for $\omega < V$,[17,19] and $h(\omega \to 0) \propto \omega \to 0$ [see Fig. 6 and Eqs. (24) and (20)], while we recover the equilibrium fluctuation-dissipation theorem $h(\omega) = 1$ for $\omega > V$, in agreement with the results found in Ref. 17. However, as the system moves deeply to the localized phase, the above deviation gets smaller and finally the equilibrium fluctuation-dissipation

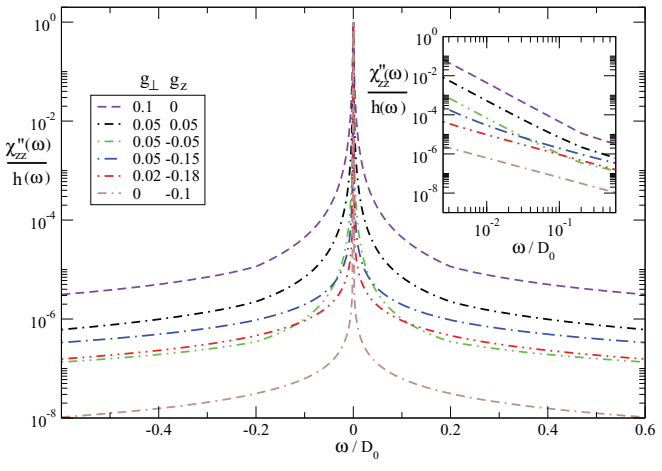

FIG. 7. (Color online) $\chi''_{zz}(\omega)/h(\omega)$ (normalized to 1) vs ω at zero temperature across the localized-delocalized KT transition. Here, $h(\omega)$ is defined in the text. The inset shows the log-log plot of $\chi''_{zz}(\omega)/h(\omega)$ (normalized to 1) vs ω. The bias voltage is fixed at $V = 0.2D_0$. Here, the bare Kondo couplings $g_{\perp,z}$ are in units of $D_0 = 1$ for all the figures.

theorem is recovered for all frequencies: $h(\omega) = 1$ for $\omega < D_0$ (see Fig. 6). To more clearly observe the singular property of $\chi''_{zz}(|\omega| = V)$, we plot the normalized Lorentzian form $\Gamma(0)\chi''_{zz}(\omega)/h(\omega) = \Gamma(\omega)\Gamma(0)/[\omega^2 + \Gamma^2(\omega)]$ (see Fig. 7). As the system moves from the delocalized to the localized phase, the width of the Lorentzian peak gets narrower and the singularity at $|\omega| = V$ gradually disappears.

V. CONCLUSIONS

In conclusion, we have calculated the zero-temperature nonequilibrium dynamical decoherence rate and charge susceptibility of a dissipative resonance-level quantum dot close to the localized-delocalized quantum phase transition. The system corresponds to a nonequilibrium anisotropic Kondo model. We generalized the previous nonequilibrium frequency-dependent RG approach approach to include the frequency dependence for the decoherence rate self-consistently. Within this generalized frequency-dependent RG approach, we calculated the dynamical decoherence rate and charge susceptibility. In the delocalized phase, both quantities exhibit singular behavior at $|\omega| = V$. In particular, the dynamical decoherence rate increases monotonically with increasing frequency. As the system cross overs to the localized phase (or effectively the ferromagnetic phase in the Kondo model), the decoherence rate at low frequencies gets progressively smaller and the singular feature is gradually smeared out, leading to a single linear frequency dependence, while the dynamical charge susceptibility shows a dip-to-peak crossover for $|\omega| < V$, indicating the crossover from the Kondo-screened to the local-moment (ferromagnetic) phase. Meanwhile, singular behaviors in dynamical decoherence rate and charge susceptibility at $\omega = \pm V$ are also smeared out in the above crossover. Furthermore, we show the deviation of the equilibrium fluctuation-dissipation theorem for small frequencies $\omega < V$, while the theorem is respected when $\omega > V$ or when the system is deeply in the localized phase. The analytical understanding of these properties is also provided. The above signatures can be used to identify experimentally the localized-delocalized quantum phase transition out of equilibrium in a dissipative quantum dot.

ACKNOWLEDGMENTS

I am grateful for helpful discussions with P. Wölfle. This work is supported by NSC Grants No. 98-2918-I-009-06 and No. 98-2112-M-009-010-MY3, the MOE-ATU program, and the NCTS of Taiwan, Republic of China.

[1] S. Sachdev, *Quantum Phase Transitions* (Cambridge University Press, Cambridge, UK, 2000).
[2] S. L. Sondhi, S. M. Girvin, J. P. Carini, and D. Shahar, Rev. Mod. Phys. **69**, 315 (1987).
[3] K. Le Hur, Phys. Rev. Lett. **92**, 196804 (2004); M.-R. Li, K. Le Hur, and W. Hofstetter, *ibid.* **95**, 086406 (2005).
[4] K. Le Hur and M.-R. Li, Phys. Rev. B **72**, 073305 (2005).
[5] L. Borda, G. Zarand, and D. Goldhaber-Gordon, e-print arXiv:cond-mat/0602019.
[6] P. Cedraschi and M. Büttiker, Ann. Phys. (NY) **289**, 1 (2001).
[7] A. Furusaki and K. A. Matveev, Phys. Rev. Lett. **88**, 226404 (2002).
[8] G. Zarand, C. H. Chung, P. Simon, and M. Vojta, Phys. Rev. Lett. **97**, 166802 (2006).
[9] E. Kim, e-print arXiv:cond-mat/0106575.
[10] S. Florens, P. Simon, S. Andergassen, and D. Feinberg, Phys. Rev. B **75**, 155321 (2007).
[11] C. H. Chung, K. Le Hur, M. Vojta, and P. Wölfle, Phys. Rev. Lett **102**, 216803 (2009).
[12] C. H. Chung, K. V. P. Latha, K. Le Hur, M. Vojta, and P. Wölfle, Phys. Rev. B **82**, 115325 (2010).
[13] S. Kirchner and Q.M. Si, Phys. Rev. Lett. **103**, 206401 (2009).
[14] G. Refael, E. Demler, Y. Oreg, and D. S. Fisher, Phys. Rev. B **75**, 014522 (2007).
[15] J. Gilmore and R. McKenzie, J. Phys. C **11**, 2965 (1999).
[16] A. Rosch, J. Paaske, J. Kroha, and P. Wölfle, Phys. Rev. Lett. **90**, 076804 (2003); A. Rosch, J. Paaske, J. Kroha, and P. Wöffle, J. Phys. Soc. Jpn. **74**, 118 (2005).
[17] S. G. Jakobs, M. Pletyukhov, and H. Schoeller, Phys. Rev. B **81**, 195109 (2010).
[18] A. Hackl, D. Roosen, S. Kehrein, and W. Hofstetter, Phys. Rev. Lett. **102**, 196601 (2009); P. Fritsch and S. Kehrein, Phys. Rev. B **81**, 035113 (2010).
[19] W. Mao, P. Coleman, C. Hooley, and D. Langreth, Phys. Rev. Lett. **91**, 207203 (2003).
[20] After bosonization and refermionization procedures, the precise form of the transverse Kondo couplings in the effective anisotropic Kondo model acquires an additional phase factor $J_\perp^{1(2)} \propto t_{1(2)} e^{i(\sqrt{2}-1/\sqrt{K})\tilde{\phi}_{s,2(1)}}$, where $\tilde{\phi}_{s,1(2)} = \sqrt{K}(\varphi_{1(2)} + \sqrt{\frac{1}{K_b}}\hat{\phi}_0)$ is the effective boson fields contributed from bosonizing the leads $c_{1(2)}(0) = \frac{1}{\sqrt{2\pi a}} F_{1(2)} e^{i\varphi_\alpha(0)}$ (where $F_{1(2)}$ is the Klein factor) and from the dissipative boson field $\hat{\phi}_0$ defined in Ref. 4. Here, $\frac{1}{K} = \frac{1}{K_b} + 1 = 1 + \alpha \equiv \frac{1}{\alpha^*}$. Since we are interested in physics close to the delocalized-localized transition, i.e., $K = \alpha^* \to 1/2$, we may therefore neglect the additional phase factor. This leads to the anisotropic Kondo model in Eq. (2). Note, however, that the additional phase factor effectively gives rise to a small shift of J_z: $J_z \to \tilde{J}_z = J_z + 1/2(\sqrt{\frac{2}{K}} - 1 - \frac{1}{2K})$, which will only give rise to a small quantitative correction to the results and will not lead to any qualitative change; C. H. Chung, K. Le Hur, M. Vojta, and P. Wölfle (in preparation).
[21] J. Paaske, A. Rosch, J. Kroha, and P. Wölfle, Phys. Rev. B **70**, 155301 (2004); J. Paaske, A. Rosch, and P. Wölfle, *ibid.* **69**, 155330 (2004).
[22] C. H. Chung and K. V. P. Latha, Phys. Rev. B **82**, 085120 (2010).
[23] H. Schmidt and P. Wölfle, Ann. Phys. (Leipzig) **19**, 160 (2010); **19**, 60 (2010).

[24]J. Paaske, A. Rosch, P. Wölfle, N. Mason, C. M. Marcus, and J. Nygard, Nature Phys. **2**, 464 (2006).

[25]D. Berman, N. B. Zhitenev, R. C. Ashoori, H. I. Smith, and M. R. Melloch, J. Vac. Sci. Technol. B **15**, 2844 (1997); D. Berman, N. B. Zhitenev, R. C. Ashoori, and M. Shayegan, Phys. Rev. Lett. **82**, 161 (1999); K. W. Lehnert, B. A. Turek, K. Bladh, L. F. Spietz, D. Gunnarsson, P. Delsing, and R. J. Schoelkopf, *ibid.* **91**, 106801 (2003).

[26]P. Fritsch and S. Kehrein, Ann. Phys. (NY) **324**, 1105 (2009).

[27]A. Mitra and A. J. Millis, Phys. Rev. B **72**, 121102(R) (2005).